PCCP

Accepted Manuscript

ROYAL SOCIETY OF CHEMISTRY

www.rsc.org/pccp

Journal Name

ARTICLE TYPE

Cite this: DOI: 10.1039/xxxxxxxxxx

Spectral assignments at infrared absorption region and anomalous thermal hysteresis in interband electronic transition of vanadium dioxide films†

Peng Zhang,[a] Mengjiao Li,[a] Qinglin Deng,[a] Jinzhong Zhang,[a] Jiada Wu,[b] Zhigao Hu,*[a] and Junhao Chu [a]

Received Date
Accepted Date

DOI: 10.1039/xxxxxxxxxx

www.rsc.org/journalname

The metal-insulator transition (MIT) is of key importance for understanding the fundamental electronic interaction that determines the physical properties of vanadium dioxide (VO_2) film. Here, the spectral slope of transmittance and reflectance at infrared absorption region (about 0.62-1.63 eV) and the interband electronic transition for VO_2 film with thickness of 27, 40 and 63 nm has been investigated. The potential applications of the spectral slope was presented in detail. It is found that the variation of resistivity and transmittance increases with the spectral slope of transmittance and reflectance. It is surprised that the resistivity for the VO_2 film with thickness of 27 nm is larger than that for the VO_2 film with thickness of 40 nm at metal state. In addition, an anomalous counterclockwise thermal hysteresis from interband electronic transition with higher energy was also found during the MIT process for the thinnest film. It is believed that this remarkable phenomenon can be related to the correlation effects in the rutile phase, which could lead to the splitting of the a_{1g} band into Hubbard bands. The lower Hubbard band would result in the electronic transition blue-shift with the empty e_g^{σ} band, which can explain the origin of the counterclockwise thermal hysteresis and abnormal resistivity at the metal state.

1 Introduction

Vanadium dioxide (VO_2) is a paradigmatic example of a prototype correlated electron system that is vital to both fundamental physics and applications. It is generally known that the VO_2 shows an unusual first-order metal-insulator transition (MIT) around room temperature with a variation in electrical conductivity of several orders of magnitude.[1,2] Furthermore, a change of lattice structure from a high temperature, rutile ($P4_2/mn$) to a low temperature, monoclinic ($P2_1/c$) has been observed during the MIT process.[3,4] Several models have been proposed to account for the origin of the MIT process. The mechanism of the MIT can be electronically (Mott transition), structurally (Peierls transition) or collaborative (Mott-Peierls transition) driven, which is usually be associated with electronic ordering phenomenon.[5–7] Because of the complicated relationship among the electron-lattice coupling and electron-electron interaction, the origin and fundamental mechanism driving the transition is still under controversial.

Due to the prominent optical and electrical properties, VO_2 is a promising candidate for a variety of applications, such as sensor devices, modulator, optical and electrical switching[8–10,12] The MIT properties could be manipulated by not only temperature, but also electric field, strain, doping and pressure et al..[13–16] In the past several decades, the impact of the above factors to the internal mechanism of MIT has been studied widely. A lot of interesting and new phenomena were found through various kinds of measurement techniques. However, the effect from the thickness on the energy transition was often ignored and scarcely investigated. It is well known that the dynamics of the electronic correlations may substantially differ from the conventional physics when the film thickness is relatively thin. The interband transitions can be affected by altering the film thickness, which have important implications in a correlated system where Coulomb repulsion between electrons and orbital overlaps. Therefore, it is necessary to provide additional insight into the underlying mechanism of the energy transition as for the case of the film with different thickness.

In this study, the VO_2 films with different thickness were prepared by pulsed laser deposition (PLD). The spectral slope of transmittance and reflectance at infrared absorption region was elucidated in detail. It is found that the resistivity at the metal state not decreases with the film thickness, which can be ascribed to the variation of the carrier concentration. In addition,

[a] Key Laboratory of Polar Materials and Devices, Ministry of Education, Department of Electronic Engineering, East China Normal University, Shanghai 200241, China.
[b] Department of Optical Science and Engineering, Fudan University, Shanghai 200433, China.
* Tel: +86-21-54345150; Fax: +86-21-54345119; E-mail: zghu@ee.ecnu.edu.cn

an anomalous counterclockwise thermal hysteresis behavior in higher energy transition was found for the thinnest VO_2 film. It is believed that the remarkable phenomenon can be related to the correlation effects in the rutile phase, which is the origin of the abnormal resistivity and counterclockwise thermal hysteresis behavior.

2 Experimental details

2.1 Fabrication, Microstructure, optical and electrical characterizations of VO_2 films

The film was synthesized by pulsed laser deposition (PLD) technique and the systematic study of growth conditions can be found elsewhere.[17] The atomic force microscopy (AFM: Digital Instruments Icon, Bruker) was used to characterize the surface morphology of the VO_2 films. To valuate the thickness and observe the surface microscopy of the VO_2 films, the scanning electron microscopy (SEM: Philips XL30FEG) was performed. The X-ray diffraction (XRD) with Cu $K\alpha$ radiation (λ=0.1542 nm) was used to characterize the crystal structure of the films. To analyze the electric properties, the resistance as the function of the temperature with different thickness was measured by a THMSE 600 heating/cooling stage (Linkam Scientific Instruments) in the temperature range from 273 to 373 K. In order to determinate the component and valence state, X-ray photoelectron spectroscopy (XPS, AXIS Ultra^{DLD}, Japan) with Al $K\alpha$ radiation (hν=1486.6 eV) was carried out at room temperature in vacuum. The temperature-dependent transmittance spectra and near-normal incident (about 8°) reflectance spectra were recorded using a double beam ultraviolet-infrared spectrophotometer (PerkinElmer Lambda 950) at the photon energy from 0.46 to 6.52 eV (190-2650 nm).

3 Results and discussion

3.1 Microstructure analysis

Atomic force microscopy (AFM) images of the films are shown in Fig. 1 (a), (b) and (c). It can be seen that the VO_2 films include many individual grains and the size of the nanoparticle increases with film thickness. Fig. 1 (d), (e) and (f) show the high resolution scanning electron microscopy (SEM) pictures of VO_2 films, which reveals that the samples are consisting of homogeneous and continuous nanoparticle. It can be found that the size of grain also increases gradually with the film thickness, which is consistent with the results obtained from the AFM. From the cross section shapes in Fig. 1 (g), (h) and (i), the film thickness is about 27, 40 and 63 nm. Fig. 2(a) shows the XRD diffraction in regular θ-2θ scanning mode for the VO_2 film with different thickness. The peaks located at 2θ=27.92° corresponds to the (011) plane for the VO_2 films. It is found that the position of (011) peak is nearly the same with the film thickness, which manifests that the strain is almost relaxed between the interface of the film and substrate. It also can be reflected by the T_{MIT} extracted from differential hysteresis loops of the resistivity and transmittance. The full width at half maximum of (011) peaks decreases with film thickness, which illustrates that the crystal quality can be improved with the film thickness.

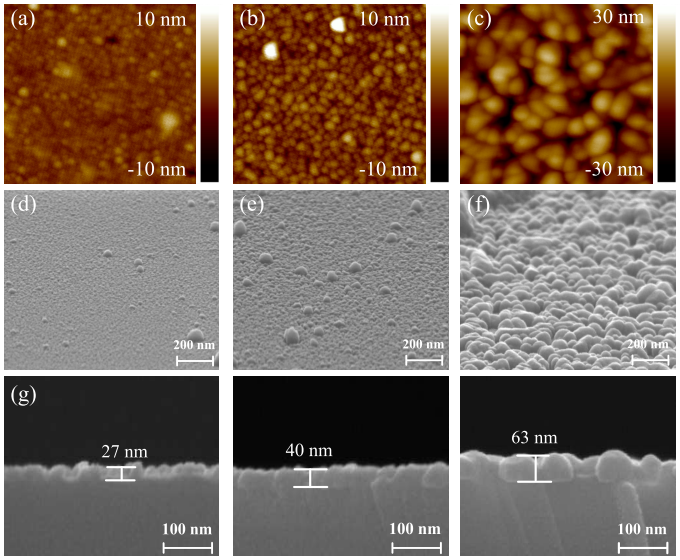

Fig. 1 (a)-(c) AFM images for the VO_2 films with 27, 40 and 63 nm. (d)-(f) The high resolution SEM pictures for VO_2 films with different thickness. (g)-(i) The cross section shapes for the films.

3.2 Electrical transport

The resistivity change during a heating-cooling cycle across the transition regime was shown in Fig. 2(b). The inset presents the differential curves of the resistivity hysteresis loops. In order to analyze and compare the transport behavior of the VO_2 films, the parameters of the electrical properties have been extracted from the related differential curves fitted by Gaussian function. Wherein the T_c represents the phase transition temperature. The discrepancy of the T_c between the heating and cooling process was defined by ΔT_c. The phase transition magnitude and the resistivity at the metal state was denoted by ΔA and R_ρ, respectively. The parameters was presented in Table I. It can be seen that the variation of the resistivity for the VO_2 film with thickness of 27, 40 and 63 nm is 133, 175 and 875, which increases with the film thickness. It is worthy noting that the resistivity drop for the VO_2 film with thickness of 27 and 40 nm is more than the magnitude of 10^2 and about 10^3 for the thickest film. The results are in good agreement with other reports for VO_2 film with different thickness.[13,18,19] Generally, the resistivity decreases at the metal state with the film thickness. However, it is confused that the resistivity at the metal state is beyond the rule for the VO_2 film with the thickness of 27 and 40 nm. It is believed that the crack or twinned structure can lead to the higher resistivity and the phase transition magnitude of the resistivity and transmittance can be reduced.[20,21] Nevertheless, the phase transition magnitude of the resistivity and transmittance increases with the film thickness, which indicates that the effect of the crack or the twinned structure can be ignored in the present work. It is generally agreed upon that the degree of the metallization is closely related with the carrier concentration. Then, the abnormal resistivity at metal state can be accounted by a large change in carrier density.

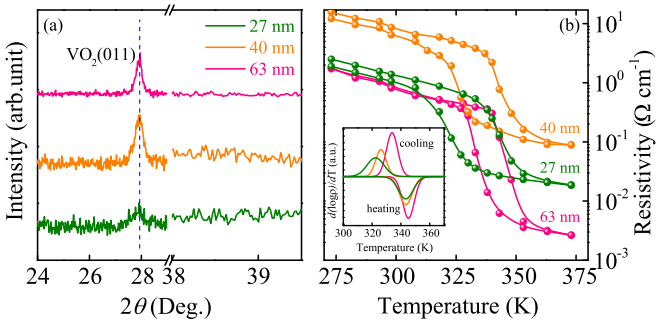

Fig. 2 (a) The θ-2θ scan XRD curves for thickness dependent VO_2 films. (b) The resistivity as the function of temperature for the VO_2 films with different thickness. The inset shows differential curves of the resistivity.

Table I. The parameters of the electrical and optical properties extracted from the related differential curves fitted by Gaussian function.

Samp.	T_c (K)	F (K)	ΔT_c (K)	ΔA	ΔTr	R_ρ	R_{Tr}
27 nm	343.4	5.08	21.1	133	0.32	0.0187	0.49
40 nm	343.4	4.46	17.3	175	0.44	0.0892	0.36
63 nm	345.2	3.94	11.4	875	0.54	0.0026	0.18

3.3 XPS survey spectra

In order to analyze the component and valence state, X-ray photoelectron spectroscopy (XPS) is carried out at room temperature in vacuum. The chemical element of C1*s* with binding energy of 285 eV was used to calibrate the spectra. The overall core level XPS survey spectra of the VO_2 film with thickness of 40 nm was shown in Fig. 3(a). The V 2*p* and O 1*s* with 2*p* doublet of the films with different thickness were presented in Fig. 3 (b)-(g). The Lorentzian-Gaussian sum function was used to dividing V 2*p* and O 1*s* peaks, which can be used to evaluate the chemical state and stoichiometry of the film.[22,23] From the V $2p_{2/3}$ peaks, it can be found that two peaks located at about 515.5 and 516.9 eV, which can be assigned to the oxidation state of V^{4+} and V^{5+}, respectively.[10,11,25,26] The observation of V^{5+} peaks is not surprised as the XPS is a surface characterization technique. In addition, the variation of the annealing condition also affects the formation of valence state and the VO_2 film surface is prone to oxidation after being exposed to atmosphere. The main peak located at about 530 eV can be assigned to O 1*s* and the additional components with O 1*s* located at about 531.5 eV can be assigned to the C-O and C=O bonds, which may come from the surface adsorption oxygen or the sample preparation process.[22] To estimate the concentrations of atoms and the stoichiometry in a homogeneous system, the general relation was used:[24]

$$N_{V^{4+}} = \frac{A_{V^{4+}}F_{V^{5+}}}{A_{V^{4+}}F_{V^{5+}} + A_{V^{5+}}F_{V^{4+}}}. \quad (1)$$

$$N_{V^{5+}} = \frac{A_{V^{5+}}F_{V^{4+}}}{A_{V^{4+}}F_{V^{5+}} + A_{V^{5+}}F_{V^{4+}}}. \quad (2)$$

$$R_{O/V} = \frac{A_{O1s}F_{O1s}}{A_{V2p_{3/2}}F_{V2p_{3/2}}}. \quad (3)$$

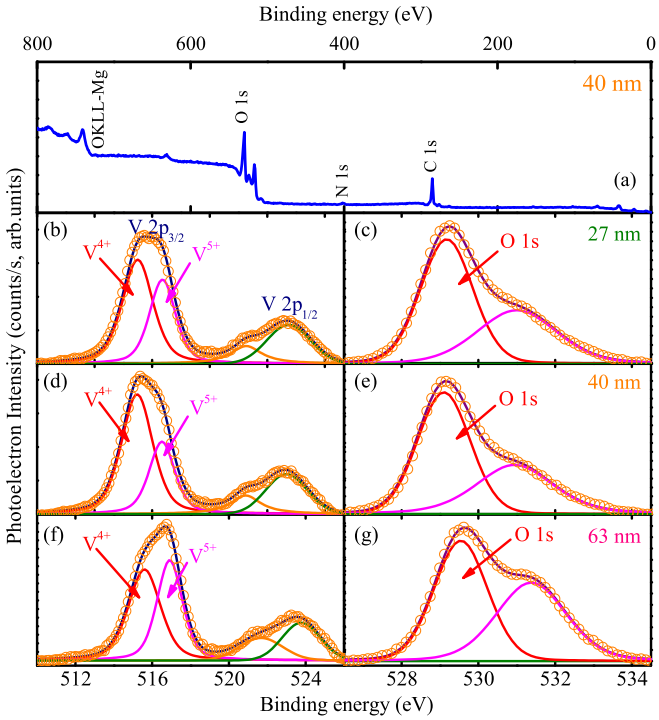

Fig. 3 (a) Overall core level XPS spectra for the VO_2 film with thickness of 40 nm. (b)-(f) XPS spectra of V 2p lines and O 1s lines with the Lorentzian-Gaussian dividing peak analysis for the VO_2 films with thickness of 27, 40 and 63 nm, respectively.

Where *A* is the peak intensity of the atom, *F* is the sensitivity factor. The *N* and *R* is the atomic concentration and the V:O ratio. Note that the $F_{V^{4+}}$ and $F_{V^{5+}}$ have been taken as the same (F=1). The $F_{V2p_{3/2}}$ and F_{O1s} is 1.3 and 0.66, respectively. Through the calculation by the equations, the stoichiometry is $VO_{1.965}$, $VO_{1.943}$ and $VO_{1.955}$ for VO_2 film with the thickness of 27, 40 and 63 nm, respectively. The V^{4+} and V^{5+} valences were evaluated with the fraction percentages of 61.8% and 38.2%, 63% and 37%, 60.3% and 39.7%, respectively. It is found that the stoichiometry and the percentages of V^{4+} and V^{5+} agree with each other for the three films, which indicates that the compositional homogeneity is almost the same.

3.4 Optical properties and electronic structures

3.4.1 NIR-UV transmittance spectra.

Fig. 4(a), (b) and (c) show the temperature-dependent transmittance changes of the VO_2 film with different thickness. The variation of the transmittance (ΔTr) at selected incident photon energies ($h\nu$=0.468 eV, λ=2650 nm) during the heating process is 0.32, 0.44 and 0.54, respectively. The variation of the transmittance increases gradually with the film thickness, which is in good agreement with the resistivity variation in Fig. 2 (b). In order to visualization the transmittance change, the hysteresis loops of transmittance at the wavelength of 2650 nm was shown in Fig. 4(e). The differential curves of the transmittance hysteresis loops are shown in Fig. 4(h), from which the T_{MIT} is about 338 K, 339 K and 341 K and the full width at half maximum decrease with

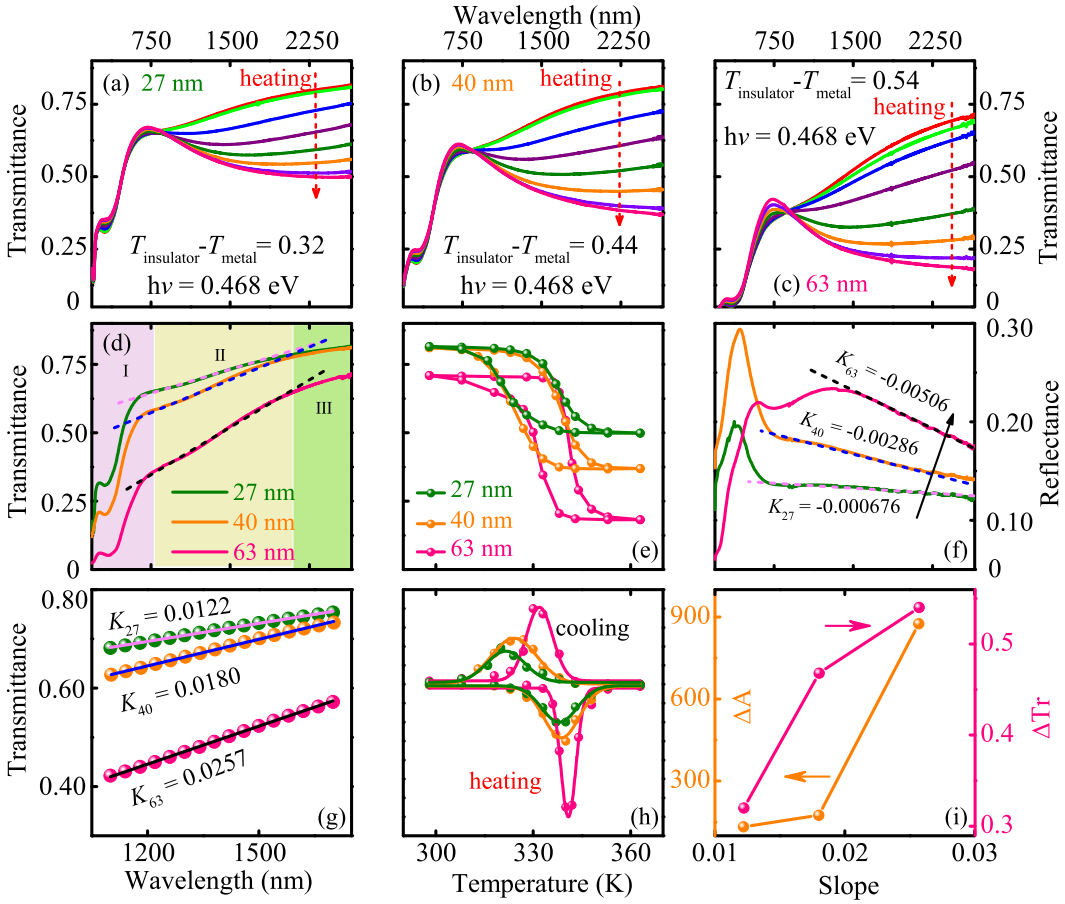

Fig. 4 (a)-(c) The transmittance spectra for the VO_2 films with different thickness. (d) The room temperature transmittance for the films with different thickness. (e) and (h) show the hysteresis loops for temperature dependence of transmittance at wavelength of 2650 nm and the differential curves, respectively. (f) The reflectance spectra for the VO_2 films with different thickness. (g) The fitting curves of the transmittance at infrared region. (i) The relationship between the spectral slope and the variation of transmittance and resistivity.

the film thickness. It should be noted that the transmittance at the metal state (R_{Tr}) is 0.49, 0.36 and 0.18 for VO_2 film with the thickness of 27, 40 and 63 nm, which indicates that the degree of the metallization increases with the film thickness. However, It was found that the degree of metallization reflected by the transmittance at the metal state is not consistent with that for the electrical behavior. For comparing the variation trend of the resistivity and transmittance at the metal state, the relevant parameters was listed in Table I.

3.4.2 NIR-UV reflectance spectra and spectral slope at infrared absorption region.

The room temperature transmittance shown in Fig. 4(d) are collected together to compare the slope of the spectra. The transmittance spectra was divided into three ranges, which is ultraviolet-visible (190-760 nm, 6.52-1.63 eV) region (defined by I), near-infrared absorption (760-2000 nm, 1.63-0.62 eV) region (defined by II) and infrared (2000-2650 nm, 0.62-0.46 eV) region (defined by III). It can be seen that the main difference of the spectra at Section III is the variation of the transmittance. The shape and variation trend of the spectra has little discrepancy. In Section I, the change of the transmittance is unconspicuous. In Section II, the divergence of the transmittance and variation trend of the spectra is obvious, especially the condition for the thickest VO_2 film with 63 nm. It can be found that the slope of the spectra in area II increases with the film thickness. The transmittance spectra in region II can be equivalent to a straight line. The fitting results are shown in Fig. 4(g). The slope of the spectra is 0.0122, 0.0180 and 0.0257 for the VO_2 film with thickness of 27, 40 and 63 nm, respectively. Based on the XRD data, transport behavior and the transmittance hysteresis loops, it can be concluded that the spectral slope in near-infrared absorption region have a positive correlations with the phase transition magnitude of the resistivity and transmittance for the VO_2 film with different thickness. In addition, the similar phenomenon also can be observed by the room temperature reflectance for the three film, which was shown in Fig. 4(f). Furthermore, from the transmittance done by Li at al.,[27] the spectral slope also has a positive correlation with the variation of the transmittance for the film with different thickness.

Fig. 4(i) presents the relationship between the spectral slope and ΔA and ΔTr. It can be found that the ΔA and ΔTr increase with the slope, which indicates that the spectral slope has a positive correlation with the variation of the transmittance and resistivity for the VO_2 film with different thickness. Therefore, it can be

Table II. Parameters of the Drude-Lorentz (DL) model for the VO_2 films extracted from the best fitting transmittance spectra at several temperatures. The 90% confidence limits are given in parentheses.

Samp.	27 nm		40 nm		63 nm	
T (K)	298	363	298	363	298	363
A_1	1.54 (0.01)	5.82 (0.22)	1.37 (0.01)	4.96 (0.15)	1.26 (0.03)	6.22 (0.12)
B_1 (eV)	1.55 (0.02)	0.93 (0.01)	1.30 (0.01)	0.90 (0.01)	0.972 (0.02)	0.91 (0.01)
E_1 (eV)	1.23 (0.01)	0.67 (0.02)	1.25 (0.01)	0.65 (0.01)	1.22 (0.01)	0.67 (0.01)
A_2	3.32 (0.01)	2.57 (0.04)	2.97 (0.05)	2.38 (0.06)	5.28 (0.04)	3.36 (0.06)
B_2 (eV)	2.17 (0.02)	1.81 (0.06)	1.91 (0.04)	1.52 (0.04)	2.09 (0.02)	1.39 (0.03)
E_2 (eV)	3.61 (0.01)	3.34 (0.01)	3.37 (0.01)	3.14 (0.01)	3.14 (0.01)	2.90 (0.01)
A_3	2.38 (0.041)	2.61 (0.13)	1.42 (0.04)	1.42 (0.02)	2.33 (0.06)	1.68 (0.03)
B_3 (eV)	1.74 (0.07)	3.35 (0.27)	4.82 (0.50)	4.43 (0.37)	4.82 (0.38)	3.93 (0.30)
E_3 (eV)	6.06 (0.02)	6.41 (0.13)	6.33 (0.12)	5.74 (0.07)	6.45 (0.13)	5.30 (0.05)
A_D	...	7.18 (0.19)	...	6.87 (0.05)	...	7.85 (0.41)
B_D (eV)	...	0.10 (0.02)	...	0.12 (0.01)	...	0.13 (0.03)

concluded that the variation trend of the electrical and optical properties can be judged conveniently from the spectral slope. It is well known that the band gap of the VO_2 film is about 0.6 eV and the transition energy from the lower V 3d filled a_{1g} band to the empty e_g^{π} band belongs to the energy range of about 0.62-1.82 eV at insulator state.[28–31] At the metal state, the a_{1g} band overlaps the e_g^{π} and the band gap is reduced to zero. That is to say, the variation of the electronic structure is mainly reflected by the change of the two bands. It is worthy noting that the energy range of region II is 1.63-0.62 eV, which is larger than the band gap while belong to the energy range of the transition between the two bands. Therefore, the degree of the phase transition can be reflected by the divergence of the transmittance in region II at insulator state.

3.4.3 Theoretical calculation of the transmittance.

It was found that the degree of metallization reflected by the electrical behavior at the metal state is not consistent with that for the transmittance. In order to investigate the abnormal phenomena, the transmittance was fitted to obtain the energy transition, A_D and B_D, which is closely related to the carrier concentration. The Drude-Lorentz (DL) oscillator dispersion relation is used to simulate the transmittance spectra, as the following

$$\varepsilon(E) = \varepsilon_{\infty} - \frac{A_D}{E^2 + iEB_D} + \sum_{k=1}^{3} \frac{A_k}{E_k^2 - E^2 - iEB_k}. \qquad (4)$$

Where ε_{∞} is the high-frequency dielectric constant. A_k, E_k, B_k and E is the amplitude, center energy, broadening of the jth oscillator and the incident photon energy, respectively. The parameter A_D is the square of the plasma frequency and B_D is the electron collision or damping frequency. The fitting parameters are listed in Table II.

It was mentioned above that the parameter A_D is the square of the plasma frequency, which is closely related to the carrier concentration n (A_D=$ne^2/\varepsilon_0\varepsilon_{\infty}m^*$). Where the ε_0 is the permittivity of free space, m^* is the conductivity effective mass. It can be taken that the A_D is proportional to the carrier concentration on the condition of unity electron average effective mass.[31–33] It is worthy noting that the B_D is nearly the same for the three VO_2 films, which indicates that the carrier mobility (μ=$e/2\pi m^*cB_D$) is

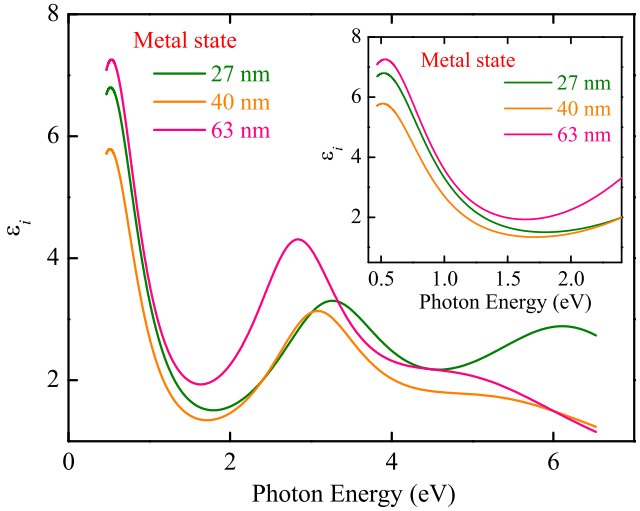

Fig. 5 The dielectric function of the VO_2 film with different thickness at metal state. The inset shows the dielectric function at infrared wavelength range.

almost identical at the metal state. The value of A_D is 7.18, 6.87 and 7.85 and B_D is 0.10, 0.12 and 0.13 for the three films, respectively. Based on the value of the A_D and B_D, it can be concluded that the overall variation of the carrier concentration increases with the film thickness. However, the value of A_D for the film with 27 nm is larger than that for the film with 40 nm, which indicates that the carrier concentration for the film with 27 nm is larger than that for the film with 40 nm. Therefore, the abnormal resistivity at the metal state can be ascribed to the variation of the carrier concentration. This also manifests that the internal mechanism reflected by the electricity and optical result at the metal state is consistent.

3.4.4 The dielectric function and comparison of the n_{eff}.

In order to increase reliability and make a contrast, we probe the phenomenon through the n_{eff}. The f-sum rule and spectral weight was used to calculate the parameter n_{eff}, the equation

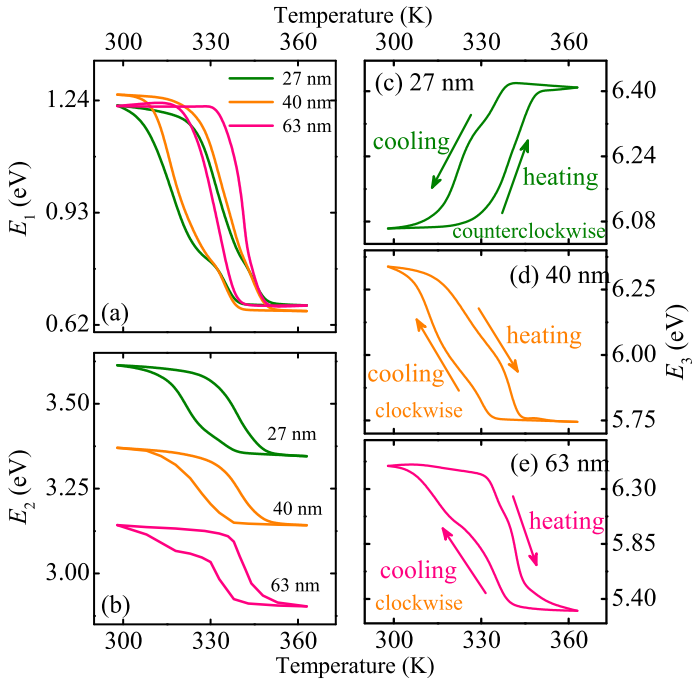

Fig. 6 (a) and (b) The electronic transition of E_1 and E_2 for the VO_2 film with different thickness, respectively. (c)-(e) The hysteresis loop of the electronic transition of E_3 for the VO_2 films.

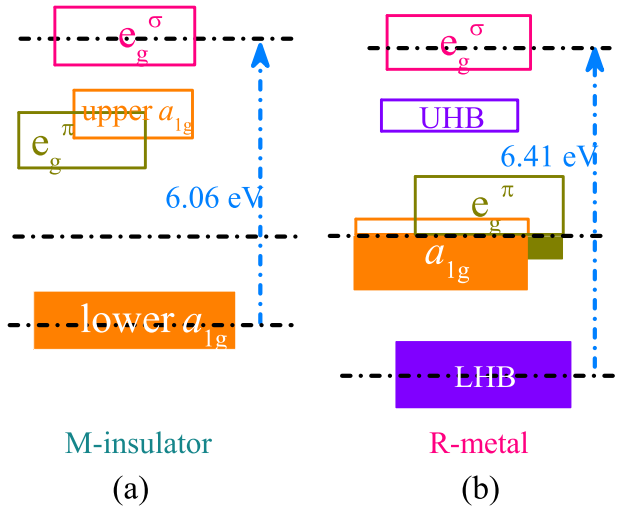

Fig. 7 (a) and (b) Schematic energy levels at the insulator and metal state for the VO_2 film with thickness of 27 nm, respectively.

can be written as the following:[31,34]

$$n_{eff}(\omega_c) = \frac{2m_0V}{\pi e^2}\int_0^{\omega_c}\sigma_r(\omega)d\omega. \quad (5)$$

Wherein $\sigma_r = \varepsilon_0\omega\varepsilon_i$ and the equation can be defined as the following form:

$$n_{eff}(\omega_c) = \frac{2\varepsilon_0 m_0\omega V}{\pi e^2}\int_0^{\omega_c}\varepsilon_i(\omega)d\omega. \quad (6)$$

Where, the σ_r and ε_i is the real part of the optical conductivity and imaginary part of the dielectric constant as a function of photon energy $\hbar\omega$, respectively. The imaginary part of the dielectric constant was shown in Fig. 5. It is believed that 95% of the spectral weight can be recovered by 4 eV, which indicates that the f-sum rule is still not fully satisfied at such high energies.[34] That is to say, the f-sum rule is appropriate for the range with lower energy. It is interesting to find that the dielectric function is sequential between the energy range of (0.47-2.37 eV) while that is chaotic beyond 2.37 eV. The energy range of 0.47-2.37 eV is within the transition energy of the filled lower a_{1g} band to the empty e_g^π band or the empty upper a_{1g} band during the MIT process. We believe that the regular result is not coincidence rather than the manifestation of the overlapping of a_{1g} band with e_g^π band. The similar phenomenon also can be observed from the spectral slope at the near-infrared absorption region. If the n_{eff} increases with the film thickness, the dielectric function will be presented at a regularity in a certain energy range. Therefore, the dielectric function was divided into two segments, which is the range with energy of (0.47-2.37 eV) and (2.37-6.53 eV).

Because the f-sum rule is not satisfied at higher energy and the n_{eff} is closely related to the variation of the a_{1g} and e_g^π band, the dielectric function with the energy range at 0.47-2.37 eV was used to compare the n_{eff} for the three films. The inset presents the dielectric function at infrared range. We assume the $f_1(\omega_c)$, $f_2(\omega_c)$ and $f_3(\omega_c)$ represent the dielectric function at the certain energy for the VO_2 film with thickness of 27, 40 and 63 nm, respectively. Obviously, the relationship of the dielectric function is $f_3(\omega_c) > f_1(\omega_c) > f_2(\omega_c)$ at the energy range of 0.47-2.37 eV. Based on Eq. (6), the relationship of the n_{eff} is $n_{eff3} > n_{eff1} > n_{eff2}$ at the certain energy range. Where the volume V can be taken as 1/2 at the metal state.[33] Through the internal mechanism obtained by transmittance spectra, it can be concluded that the peculiar resistivity at the metal state can be attributed to the variation of the carrier concentration. Generally, the carrier concentration will be increased with the film thickness. Then, it is confused that the carrier concentration of the film with thickness of 27 nm is larger than that for the film with thickness of 40 nm. It was believed that the occurrence of the Hubbard band may be the sign of the increased overlapping of the a_{1g} band to the e_g^π band.[34]

3.5 Electronic transition and band structure

From the fitting results, three center energies can be assigned to the following electronic transitions:[36] (1) lower $V3d$ filled a_{1g} band to the empty e_g^π band (E_1); (2) the filled $O2p$ band to the empty e_g^π band (E_2); (3) lower $V3d$ filled a_{1g} to the empty e_g^σ band (E_3). In this study, the E_1 and E_2 present the conventional thermal hysteresis as a function of temperature, which are shown in Fig. 6 (a) and (b). However, an abnormal hysteresis was found for the thinnest film with thickness of 27 nm. The hysteresis loop of the electronic transition of E_3 was shown in Fig. 6 (c), (d) and (e). Surprisingly, it can be found that the E_3 exhibits counterclockwise hysteresis loop for the thinnest film while the E_3 show clockwise hysteresis loop for the other two films. The similar phenomenon was previously found in magnetization and resistivity of $La_{1-x}Sr_xMnO_3$.[35] They believed that the abnormal thermal hysteresis can be attributed by the competing interaction of different metal

phases. According to the conventional band theory, the lower and upper Hubbard bands (LHB and UHB, respectively) was not considered. Correlation effects in the rutile phase could lead to a degree of splitting of the a_{1g} into lower and upper Hubbard bands.[37] It was believed that the Hubbard bands play a key role in the prominence of the pseudogap-type transition from the filled a_{1g} band to the empty e_g^π band.[34] In addition, the lower Hubbard band has been seen previously in photoemission experiments on bulk VO_2.[38]

The E_3 is the transition of filled a_{1g} to the empty e_g^σ band at the insulator and metal state. It is well known that the a_{1g} band will be shifted up during the MIT process and overlapping with the e_g^π band, which indicates that the energy of E_3 decreases with the temperature. However, the E_3 variation is contrary to the convention perspective. Taken the Hubbard band into consideration, the counterclockwise hysteresis loop can be ascribed to the Hubbard bands splitted from the a_{1g} band. The Schematic energy levels at the insulator and metal state for the VO_2 film with thickness of 27 nm were shown in Fig. 7 (a) and (b). Assuming the splitting of the a_{1g} band continuous during the MIT process, the lower Hubbard band will shift down and keep steady state at the metal state. This will lead to the transition energy of E_3 blue-shift during the MIT process. Therefore, the counterclockwise hysteresis behavior can be observed. Taken the thickness of the film, we believe the correlation effects are more easily influenced by the interfacial effect for the thinnest film. Furthermore, the occurrence of the Hubbard bands may symbolize the increased overlapping of the a_{1g} band to the e_g^π band, which may be the origin of the abnormal resistivity at the metal state. Therefore, the counterclockwise hysteresis loop of E_3 can be observed for the VO_2 film with thickness of 27 nm.

4 Conclusions

In summary, it was found that the spectral slope in near-infrared absorption region have a positive correlations with the phase transition magnitude of the resistivity and transmittance for the VO_2 film with different thickness. The finding is of benefit to discern and forecast the optical and electrical properties of film from the macroscopic level. In addition, the abnormal resistivity at the metal state was observed. The parameters of Drude model and the f-sum rule were applied to account for the phenomena, which can be attributed to the variation of the carrier concentration. Remarkably, the E_3 energy exhibits a counterclockwise hysteresis loop with temperature for the VO_2 with thickness of 27 nm, which can be ascribed to the occurrence of the Hubbard bands. It was believed that the lower Hubbard band may lead to the transition of E_3 blue shift and symbolize the increased overlapping of the a_{1g} band to the e_g^π band.

5 Acknowledgment

This work was financially supported by Major State Basic Research Development Program of China (Grant Nos. 2013CB922300 and 2011CB922200), the Natural Science Foundation of China (Grant Nos. 11374097 and 61376129), Projects of Science and Technology Commission of Shanghai Municipality (Grant Nos. 15JC1401600, 14XD1401500, 13JC1402100, and 13JC1404200), and the Program for Professor of Special Appointment (Eastern Scholar) at Shanghai Institutions of Higher Learning.

References

1 F. J. Morin, *Phys. Rev. Lett.*, 1959, **3**, 34-36.
2 P. Baum, D. S. Yang and A. H. Zewail, *Science*, 2007, **318**, 788-792.
3 C. Kubler, H. Ehrke, R. Huber, R. Lopez, A. Halabica, R. F. Haglund and A. Leitenstorfer, *Phys. Rev. Lett.*, 2007, **99**, 99, 116401.
4 D. Wegkamp, M. Herzog, L. Xian, M. Gatti, P. Cudazzo, C. L. McGahan, R. E. Marvel, R. F. Haglund, Jr., A. Rubio, M. Wolf and J. Sthler, *Phys. Rev. Lett.*, 2014, **113**, 216401.
5 R. M. Wentzcovitch, W. W. Schulz and P. B. Allen, *Phys. Rev. Lett.*, 1994, **72**, 3389.
6 T. M. Rice, H. Launojs and J. P. Pouget, *Phys. Rev. Lett.*, 1994, **73**, 3042.
7 M. M. Qazilbash, M. Brehm, B. G. Chae, P. C. Ho, G. O. Andreev, B. J. Kim, S. J. Yun, A. V. Balatsky, M. B. Maple, F. Keilmann, H. T. Kim and D. N. Basov, *Science*, 2007, **318**, 1750-1753.
8 L. Pellegrino, N. Manca, T. Kanki, H. Tanaka, M. Biasotti, E. Bellingeri, A. S. Siri and D. Marre, *Adv. Mater.*, 2012, **24**, 2929-2934.
9 N. Shukla, A. V. Thathachary, A. Agrawal, H. Paik, A. Aziz, D. G. Schlom, S. K. Gupta, R. E. Herbert and S. Datta, *Nat. Commun.*, 2015, **6**, 7812.
10 Y. Zhou, J. Park, J. Shi, M. Chhowalla, H. Park, D. A. Weitz and S. Ramanathan, *Nano Lett.*, 2015, **15**, 1627-1634.
11 S. Chen, J. J. Liu, L. H. Wang, H. J. Luo, Y. F. Gao, *J. Phys. Chem. C.*, 2014, **118**, 18938-18944.
12 A. Tselev, J. D. Budai, E. Strelcov, J. Z. Tischler, A. Kolmakov and S. V. Kalinin, *Nano Lett.*, 2011, **11**, 3065-3073.
13 B. A. Nagaphani, X. G. Alexander, D. Marc, C. Matteo, G. Li, H. R. Alexander, K. Roopali, O. Hendrik, A. J. Catherine, A. Elke, P. R. Kevin, A. U. Hermann, G. S. Mahesh and S. P. P. Stuart, *Nat. Phys.*, 2013, **9**, 661-666.
14 T. X. Nan, M. Liu, W. Ren, Z. G. Ye and N. X. Sun, *Sci. Rep.*, 2012, **4**, 5931.
15 C. Marini, E. Arcangeletti, D. D. Castro, L. Baldassare, A. Perucchi, S. Lupi, L. Malavasi, L. Boeri, E. Pomjakushina, K. Conder and P. Postorino, *Phys. Rev. B*, 2008, **77**, 235111.
16 L. G. Bai, Q. Li, S. A. Corr, Y. Meng, C. Y. Park, S. V. Sinogeikin, C. Ko, J. Q. Wu and G. Y. Shen, *Phys. Rev. B*, 2015, **91**, 104110.
17 P. Zhang, K. Jiang, Q. L. Deng, Q. H You, J. Z. Zhang, J. D. Wu, Z. G. Hu and J. H. Chu, *J. Mater. Chem. C*, 2015, **3**, 5033-5040.
18 D. Brassard, S. Fourmaux, M. J. Jacques, J. C. Kieffer and M. A. El Khakani, *Appl. Phys. Lett.*, 2005, **87**, 051910.
19 R. Molaei, R. Bayati, F. Wu and J. Narayan, *J. Appl. Phys.*, 2014, **115**, 164311.
20 K. Nagashima, T. Yanagida, H. Tanaka and T. Kawai, *Phys. Rev. B*, 2006, **74**, 172106.

21 X. Li, A. Gloter, H. Gu, X. Cao, P. Jin and C. Colliex, *Acta Mater.*, 2013, **61**, 6443-6452.

22 S. Rathi, I. Lee, J. H. Park, B. J. Kim, H. T. Kim and G. H. Kim, *ACS Appl. Mater. Interfaces*, 2014, **6**, 19718-19725.

23 Z. Yang and S. Ramanathan, *Appl. Phys. Lett.*, 2011, **98**, 192113.

24 Q. W. Shi, W. X. Huang, Y. X. Zhang, J. Z. Yan, Y. B. Zhang, M. Mao, Y. Zhang and M. J. Tu, *ACS Appl. Mater. Interfaces*, 2011, **3**, 3523-3527.

25 N. F. Quackenbush, J. W. Tashman, J. A. Mundy, S. Sallis, H. Paik, R. Misra, J. A. Moyer, J. H. Guo, D. A. Fischer, J. C. Woicik, D. A. Muller, D. G. Schlom and L. F. J. Piper, *Nano Lett.*, 2013, **13**, 4857-4861.

26 C. H. Chen and Z. Y. Fan, *Appl. Phys. Lett.*, 2009, **95**, 262106.

27 M. Li, X. Wu, L. Li, Y. X. Wang, D. B. Li, J. Pan, S. J. Li, L. T. Sun and G. H. Li, *J. Mater. Chem. A*, 2014, **2**, 4520-4523.

28 W. T. Liu, J. Cao, W. Fan, Z. Hao, M. C. Martin, Y. R. Shen, J. Wu and F. Wang, *Nano Lett.*, 2011, **11**, 466-470.

29 W. W. Li, Q. Yu, J. R. Liang, K. Jiang, Z. G. Hu, J. Liu, H. D. Chen and J. H. Chu, *Appl. Phys. Lett.*, 2011, **99**, 241903.

30 A. Gavinit and C. C. Y. Kwan, *Phys. Rev. B*, 1972, **5**, 3138.

31 H. W. Verleur, A. S. Barker and C. N. Berglund, *Phys. Rev.*, 1968, **172**, 788-798.

32 K. Okazaki, H. Wadati, A. Fujimori, M. Onoda, Y. Muraoka and Z. Hiroi, *Phys. Rev. B*, 2004, **69**, 165104.

33 D. B. Mcwhan, M. Marezio, J. P. Remeika and P. D. Dernier, *Phys. Rev. B*, 1974, **10**, 490.

34 T. J. Huffman, P. Xu, A. J. Hollingshad, M. M. Qazilbash, Lei Wang, R. A. Lukaszew, S. Kittiwatanakul, J. Lu and S. A. Wolf, *Phys. Rev. B*, 2015, **91**, 205140.

35 J. Dho, W. S. Kim and N. H. Hur, *Phys. Rev. Lett.*, 2001, **87**, 187201.

36 W. W. Li, J. J. Zhu, X. F. Xu, K. Jiang, Z. G. Hu, M. Zhu and J. H. Chu, *J. Appl. Phys.*, 2011, **110**, 013504.

37 S. Biermann, A. Georges, A. Lichtenstein and T. Giamarchi, *Phys. Rev. Lett.*, 2001, **87**, 276405.

38 T. C. Koethe, Z. Hu, M. W. Haverkort, C. S. Langeheine, F. Venturini, N. B. Brookes, O. Tjernberg, W. Reichelt, H. H. Hsieh, H. J. Lin, C. T. Chen and L. H. Tjeng, *Phys. Rev. Lett.*, 2006, **97**, 116402.

Graphical contents entry. From Fig. (a) and (b), it was found that the spectral slope at infrared absorption region increases with film thickness. Due to the effect of the Hubbard band in Fig. (c), it will lead to the E_3 blue-shift and keep steady at metal state for thinnest film.